HHS Public Access

Author manuscript

J Bone Miner Res. Author manuscript; available in PMC 2017 May 01.

Published in final edited form as:

J Bone Miner Res. 2016 May ; 31(5): 1030–1040. doi:10.1002/jbmr.2776.

Sclerostin antibody treatment improves the bone phenotype of *Crtap*$^{-/-}$ mice, a model of recessive Osteogenesis Imperfecta

Ingo Grafe[1], **Stefanie Alexander**[1], **Tao Yang**[1,a], **Caressa Lietman**[1], **Erica P Homan**[1], **Elda Munivez**[1], **Yuqing Chen**[1,2], **Ming Ming Jiang**[1], **Terry Bertin**[1], **Brian Dawson**[1,2], **Franklin Asuncion**[3], **Hua Zhu Ke**[4], **Michael S Ominsky**[3], and **Brendan Lee**[1,2]

[1]Department of Molecular and Human Genetics, Baylor College of Medicine, Houston, TX, USA

[2]Howard Hughes Medical Institute, Houston, TX, USA

[3]Department of Metabolic Disorders, Amgen, Inc., Thousand Oaks, CA, USA

[4]UCB Pharma, Slough, UK

Abstract

Osteogenesis Imperfecta (OI) is characterized by low bone mass, poor bone quality and fractures. Standard treatment for OI patients is limited to bisphosphonates, which only incompletely correct the bone phenotype, and seem to be less effective in adults. Sclerostin neutralizing antibodies (Scl-Ab) have been shown to be beneficial in animal models of osteoporosis, and dominant OI resulting from mutations in the genes encoding type I collagen. However, Scl-Ab treatment has not been studied in models of recessive OI. Cartilage associated protein (CRTAP) is involved in posttranslational type I collagen modification, and its loss of function results in recessive OI. In this study, we treated 1 and 6 week old *Crtap*$^{-/-}$ mice with Scl-Ab for 6 weeks (25 mg/kg, s.c., twice per week), to determine the effects on the bone phenotype in models of "pediatric" and "young adult" recessive OI. Vehicle treated *Crtap*$^{-/-}$ and wildtype (WT) mice served as controls. Compared with control *Crtap*$^{-/-}$ mice, microCT analyses showed significant increases in bone volume and improved trabecular microarchitecture in Scl-Ab treated *Crtap*$^{-/-}$ mice in both age cohorts, in both vertebrae and femurs. Additionally, Scl-Ab improved femoral cortical parameters in both age cohorts. Biomechanical testing showed that Scl-Ab improved parameters of whole bone strength in *Crtap*$^{-/-}$ mice, with more robust effects in the week 6–12 cohort, but did not affect the increased bone brittleness. Additionally, Scl-Ab normalized the increased osteoclast numbers, stimulated bone formation rate (week 6–12 cohort only), but did not affect osteocyte

Corresponding author: Brendan Lee, M.D., Ph.D., Department of Molecular and Human Genetics, Baylor College of Medicine, One Baylor Plaza, R815, Houston, Texas, 77030, USA, Phone: 713-798-5443, FAX: 713-798-5168, blee@bcm.edu.
[a]current address: Laboratory of Skeletal Biology, Center for Skeletal Diseases and Tumor Metastasis, Van Andel Research Institute, Grand Rapids, MI 49503.

Disclosures: Franklin Asuncion and Michael S Ominsky are employees of Amgen Inc, Hua Zhu Ke is an employee of UCB Pharma. The other authors have no conflict of interest to declare.

Authors' roles: Study design: IG, TY, HZK, MSO, BL. Experimental conduct: IG, SA, TY, CL, EPH, EM, YC, MMJ, TB, BD, FA. Data collection: IG, SA, CL, EPH, EM, TB, BD, FA. Data analysis: IG, SA, CL, FA. Data interpretation: IG, FA, HZK, MSO, BL. Drafting manuscript: IG, SA, CL, EPH, TB, FA, MSO, BL. Revising manuscript: All authors. Approving final version of manuscript: All authors. IG and BL take responsibility for the integrity of the data analysis.

Supplemental figures Fig.S1 and Fig.S2 have been included with the submission.

density. Overall, our findings suggest that Scl-Ab treatment may be beneficial in the treatment of recessive OI caused by defects in collagen post-translational modification.

Keywords

Osteogenesis Imperfecta; Anabolic Therapeutics; Preclinical Studies; Bone QCT/microCT; Bone histomorphometry

Introduction

Osteogenesis imperfecta (OI) is a heritable multi-system syndrome with a prominent skeletal phenotype. It is characterized by low bone mass and impaired bone quality, leading to skeletal deformities and fractures, as well as extraskeletal manifestations (1). About 90% of the cases are caused by autosomal dominant mutations in the genes encoding type I collagen (*COL1A1* and *COL1A2*), the major component of the bone matrix (1–2). Recessively inherited OI can be caused by mutations in a variety of genes, including members of the prolyl-3-hydroxylation (P3H) complex, which is involved in post-translational modification and processing of type I procollagen (2–3). This complex is located in the rough endoplasmatic reticulum and consists of prolyl 3-hydroxylase 1 (P3H1, encoded by *LEPRE1*), cartilage-associated protein (CRTAP, encoded by *CRTAP*), and cyclophilin B (CypB, encoded by *PPIB*). It catalyzes the 3-hydroxylation of a single proline in the alpha 1 chain of type I procollagen, and functions as a collagen chaperone and isomerase (3–5). Mutations in any member of the P3H complex can cause moderate to severe or lethal OI in humans (5–8), and mutations in *CRTAP* or *LEPRE1* have been identified in up to 24% of OI patients without OI-causing mutations in *COL1A1/COL1A2* (6).

In children with OI, the current standard of pharmacological treatment (1) is antiresorptive bisphosphonates, which increase bone mineral density (BMD) (9–15) and growth (12). However, a fracture reduction by bisphosphonates in OI has not consistently been shown in all studies (13–15). Additionally, bisphosphonates seem to be less effective in the appendicular skeleton (16) and in the treatment of adult OI patients (15,17–18). More recently, denosumab, an antibody that inhibits Receptor activator of NF-κB ligand (RANKL) and thereby inhibits osteoclast formation and bone resorption, has been found to increase BMD in case series of OI patients (19–20); however, no controlled studies and long-term data are currently available regarding the effectiveness and safety of denosumab in OI. The only currently available osteoanabolic drug approved for the treatment of osteoporosis is intermittent parathyroid hormone (PTH (1–34); Teriparatide (TPD)) (21). Although effective in increasing BMD and reducing fracture risk in patients with osteoporosis, a recent trial in adult OI patients found that TPD increased the BMD in patients with mild OI, but not in moderate to severe forms of OI and did not significantly reduce the amount of self-reported fractures (22). Moreover, due to an increased osteosarcoma incidence observed in rats receiving PTH (1–34), TPD therapy is limited to 2 years and not approved for pediatric treatment (23).

Inhibition of sclerostin, a product of the SOST gene and a negative regulator of bone mass, may provide a new therapeutic avenue to improve skeletal health in OI patients. Sclerostin is

secreted predominantly by osteocytes (24–25), and antagonizes canonical Wnt/β-catenin signaling in osteoblasts (26), resulting in the inhibition of osteoblastogenesis and bone formation (27–28). Antibodies targeted to inhibit sclerostin (Scl-Ab) improved bone formation and bone mass in animal studies including models of post-menopausal osteoporosis (29), and age- (30) and immobility-related bone loss (31), supporting a benefit of sclerostin inhibition in low bone mass disorders. In human clinical phase I and II trials, sclerostin antibodies induced robust increases in BMD, suggesting a promising new option for the treatment of osteoporosis (32–34).

The efficacy of sclerostin inhibition in OI has previously been tested in mouse models of dominant OI (35–39), and in the oim/oim model of recessive OI due to a mutation in *Col1a2* (40–41). These studies have mostly shown that Scl-Ab treatment has beneficial effects on both cortical and trabecular bone in OI. However, the effects of Scl-Ab in recessive OI due to defects in post-translational collagen modification are not known and may be distinct, considering that the different genetic and molecular mechanisms may differentially affect the response to sclerostin inhibition. *Crtap*$^{-/-}$ mice recapitulate the severe phenotype of human recessive OI caused by mutations in *CRTAP*, including altered collagen post-translational modification, osteopenia and increased bone brittleness (5,7). Additionally, *Crtap*$^{-/-}$ mice exhibit extraskeletal manifestations including skin, kidney and lung abnormalities, the latter characterized by an increased alveolar airway space (42). In this study, we tested to what extent Scl-Ab treatment can improve the bone pathology in the *Crtap*$^{-/-}$ mouse model. For this, we treated two age cohorts of *Crtap*$^{-/-}$ mice with Scl-Ab for 6 weeks as models of “pediatric” and “young adult” recessive OI, and evaluated the effects on trabecular and cortical bone, bone microarchitecture, cellular composition, bone formation and strength. Because lung abnormalities can contribute to morbidity and mortality in patients with severe OI (43–44), we additionally tested whether Scl-Ab treatment had any effect on the lung phenotype of *Crtap*$^{-/-}$ mice.

Methods

Animals, treatment and tissue collection

Crtap $^{-/-}$ (5) and wild-type (WT) mice were generated by mating *Crtap*$^{+/-}$ mice, maintained on a mixed C57BL/6 genetic background, housed in the Baylor College of Medicine Animal vivarium under a 12h light/dark cycle and provided water and standard chow ad libitum. All animal studies were performed following the approved protocol of the Animal Care and Use Committee (IACUC) at Baylor College of Medicine, Houston, TX, USA. Sclerostin neutralizing antibody (Scl-AbVI) was provided by Amgen Inc. (Thousand Oaks, CA, USA) and UCB Pharma (Slough, UK), and diluted 1:10 in phosphate-buffered saline (PBS) to 3.6 mg/ml for administration. Two age cohorts of female *Crtap* $^{-/-}$ mice were treated with Scl-Ab (25 mg/kg in PBS, s.c. twice per week) for 6 weeks: 6 week old mice were treated for 6 weeks (“wk6–12” cohort), to first assess efficacy and safety in a cohort reflecting treatment of “young adult” OI, then, 1 week old mice were treated from week 1–7 (“wk1–7” cohort), to reflect treatment of a “pediatric” cohort. Control *Crtap* $^{-/-}$ and WT mice were treated with PBS only. *Crtap* $^{-/-}$ mice were randomly assigned to Scl-Ab treatment or control group. No blinding to group assignment was possible during treatment, as Scl-Ab or PBS were injected

accordingly. For the subsequent analyses the investigators were blinded to genotype and treatment group. Calcein (15 mg/kg, I.P.) was injected 7 days and 2 days before euthanasia to assess the parameters of dynamic bone histomorphometry. Lungs of the mice were equally inflated immediately after euthanizing with 4% paraformaldehyde at a pressure of 25 cm H_2O and then suture closed at the trachea. Lungs were then gently removed from the thorax and fixed in 4% paraformaldehyde overnight. Spines and left femurs were collected, fixed in 10% formalin and processed for microCT imaging. After imaging, spines were embedded for histomorphometry. Right femurs were wrapped in saline soaked gauze and stored at −20°C for subsequent biomechanical testing.

MicroCT analyses

Spines and left femurs were scanned in 70% ethanol using a Scanco μCT-40 microCT system (55kVp and 145μA X-ray source) and scans were reconstructed at a 16μm isotropic voxel size. Trabecular bone of L4 vertebrae and the distal metaphyseal part of left femurs were analyzed using Scanco software by manually contouring trabecular bone. For vertebrae, the region of interest (ROI) was defined as the trabecular volume between the L4 vertebral endplates. At femoral trabecular ROI 75 slides (=1.2 mm) were analyzed proximal to the distal femoral growth plate in WT femurs. To not underestimate trabecular bone in *Crtap*$^{-/-}$ mice, which have shorter femurs, the number of slides defined as ROI was reduced according to femur length (67 and 64 slides for the wk6–12 and wk1–7 cohorts, respectively). Quantification of trabecular parameters was performed using the Scanco software with a threshold value of 210. These parameters include bone volume/total volume (BV/TV), trabecular number (Tb.N), trabecular thickness (Tb.Th), connectivity density (Conn.D) and tissue mineral density (TMD) (45). Femur length was measured from the top of the femoral head to the bottom of the medial condoyle. Cortical bone parameters of the femoral midshaft were measured at the exact center and at the distal 75% of femur length using the automated thresholding algorithm included in the Scanco software. Trabeculae in contact with cortical bone were manually removed from the ROI (11 slides analyzed per location, threshold 210). The cortical parameters include total cross-sectional area (Tt.Ar), cortical bone area (Ct.Ar), marrow area (Ma.Ar), cortical thickness (Ct.Th), cross-sectional moments of inertia (CSMI), anterior-posterior diameter, and tissue mineral density (TMD) (45). Seven spines and femurs were scanned per group. MicroCT imaging of the femurs revealed a healed spontaneous fracture in the femur of one control *Crtap*$^{-/-}$ mouse of the wk6–12 cohort, affecting the midshaft region, and a healed spontaneous fracture of one control *Crtap*$^{-/-}$ mouse of the wk1–7 cohort, affecting both the metaphyseal and midshaft regions. These femurs were excluded from the respective microCT quantifications. We did not observe femur fractures of WT or Scl-Ab treated *Crtap*$^{-/-}$ mice in both age cohorts.

Biomechanical testing

Right femurs were wrapped in saline soaked gauze and stored at −20°C until testing by Amgen Inc.. Whole femurs were tested in three-point bending to failure on a servohydraulic test system (MTS 858 Mini Bionix II, MTS Systems Corp., Eden Prairie). Femurs were placed on the lower supports of a three point bending fixture with the posterior side facing downward. The span between the two lower supports was set at 6 mm. Load was applied on the midpoint of the anterior surface at a constant displacement rate of 0.1 mm/sec until

failure occurred. Maximum load, stiffness, and energy absorbed were assessed from the load displacement curve within Microsoft Excel. Yield point and elastic region were determined using a 0.05 mm (wk6–12 cohort) and 0.02 mm (wk1–7 cohort) offset from the slope, to assess stiffness within the elastic region. Before testing, femurs were scanned using a eXplore Locus SP scanner (GE Healthcare, London, Ontario) and reconstructed to an isotopic voxel size of 8μm to obtain geometric data (diameter and moment of inertia) at the femoral midshaft. These were utilized to calculate the intrinsic material properties ultimate strength, toughness and elastic modulus as previously reported (46). Femurs of n=3 WT, n=5 *Crtap*$^{-/-}$ control and n=5 Scl-Ab treated *Crtap*$^{-/-}$ mice were analyzed in the wk6–12 cohort, femurs of n=9 WT, n=6 *Crtap*$^{-/-}$ control and n=6 Scl-Ab treated *Crtap*$^{-/-}$ mice were analyzed in the wk1–7 cohort.

Histomorphometry

Undecalcified lumbar spines of *Crtap* $^{-/-}$ and WT mice were embedded in methacrylate for sectioning. Then trichrome stained slides were used to quantify BV/TV, osteoblast and osteocyte parameters, and TRAP-stained slides were used to quantify osteoclast parameters of vertebral bodies L4 (n=6 per group) at 20X resolution using the Bioquant Osteo Image Analysis System version (12.1.6). Unstained sections were used for the analysis of dynamic bone formation parameters.

Measurement of TRACP5b serum levels

Blood samples were collected from mice of the wk6–12 cohort by retro-orbital bleeding under anesthesia before euthanasia, serum separated by centrifugation and stored at −80°C. TRACP5b was measured using a commercially available, species-specific ELISA kit (IDS, Fountain Hills, AZ, USA) in accordance with manufacturer's protocol. N=7 per group.

Lung histology and morphometry

Coronal sections of lungs were stained with Hematoxylin and Eosin. To quantify the distance between alveolar structures we used the mean linear intercept (MLI) method as described previously (47–48). Briefly, 10 histological fields per mouse were taken at 20X magnification from both lungs using an Axioplan 2 (Zeiss) microscope (n=8 WT, n=6 *Crtap* $^{-/-}$ control and n=6 Scl-Ab treated *Crtap* $^{-/-}$ mice). The MLI was quantified using a modified ImageJ software (National Institutes of Health). Blood vessels, large airways and other nonalveolar structures were manually removed in each image. The software then automatically thresholded alveolar tissue in the images and overlaid 1,353 lines over each images. The number of lines that ended on or intercepted alveolar tissue was used to calculate the MLI.

Statistical analyses

For comparisons between the 3 groups, we performed One Way Analysis of Variance (ANOVA) if normal distribution and equal variance of groups were confirmed, followed by all pairwise multiple comparison using the Holm-Sidak method. If the equal variance or normal distribution test failed, we performed Kruskal-Wallis One Way ANOVA on Ranks, followed by pairwise multiple comparison using the Tukey Test (if group sizes were equal)

or Dunn's methods (when group sizes were not equal). A P value <0.05 was considered statistically significant for ANOVA and Kruskal-Wallis One Way ANOVA on Ranks. To determine if differences between groups were significant for the posthoc pairwise multiple comparisons, each P value was compared to a critical level depending on the rank of the P value and the total number of comparisons. The effects of Scl-Ab in *Crtap* $^{-/-}$ mice were unknown at study start. We calculated that to detect a 50% difference in bone volume/total volume (BV/TV) between control and Scl-Ab treated *Crtap* $^{-/-}$ mice with a 90% power, a group size of n=7 mice is required. We used Sigma Plot V11.0 (Systat Software Inc.) for statistical analyses.

Results

Scl-Ab did not alter the reduced body weight of *Crtap*$^{-/-}$ mice

As previously reported, *Crtap*$^{-/-}$ mice are smaller and weigh less than wild-type (WT) mice (5). In the current study, control *Crtap*$^{-/-}$ mice in both the wk6–12 and wk1–7 cohorts weighed about 24% less than WT mice at study end. Scl-Ab treatment did not significantly alter the weight of *Crtap*$^{-/-}$ mice in both age cohorts (Fig. S1, S2). There were no obvious negative effects of Scl-Ab treatment on the *Crtap*$^{-/-}$ mice with regard to appearance, movement, or other behavior.

Scl-Ab improved trabecular bone mass and microarchitecture in spine and femur of *Crtap*$^{-/-}$ mice

As expected, at the L4 vertebral bodies control *Crtap*$^{-/-}$ mice exhibited reduced bone volume/total volume (BV/TV), trabecular number (Tb.N.), trabecular thickness (Tb.Th) and connectivity density (Conn.D) relative to WT mice of the same age (Fig. 1). By contrast, treatment of *Crtap*$^{-/-}$ mice with Scl-Ab increased BV/TV and Tb.N, and Tb.Th was no longer different from WT mice in both cohorts. Scl-Ab treatment increased the Conn.D in vertebrae of *Crtap*$^{-/-}$ mice in the wk1–7 cohort, but not in the wk6–12 cohort. Compared with WT mice, the tissue mineral density (TMD) of vertebral trabecular bone matrix was higher in 12 week old control *Crtap*$^{-/-}$ mice, but not in 7 week old *Crtap*$^{-/-}$ mice. In both age cohorts, Scl-Ab increased the TMD of *Crtap*$^{-/-}$ mice to above WT levels.

Femurs of control *Crtap*$^{-/-}$ mice showed reduced BV/TV, Tb.N and Conn.D at the metaphysis compared with WT mice in both age cohorts, while Tb.Th was not statistically different from WT mice (Fig. 2). Scl-Ab significantly improved the BV/TV and Tb.N of *Crtap*$^{-/-}$ mice in both age cohorts compared with control *Crtap*$^{-/-}$ mice, in the wk6–12 cohort these parameters were similar to WT mice. In addition, Scl-Ab significantly increased Tb.Th and Conn.D. in 12 week old *Crtap*$^{-/-}$ mice compared with control *Crtap*$^{-/-}$ mice, but did not significantly affect these parameters in the wk1–7 cohort. The TMD of trabecular femoral bone in control *Crtap*$^{-/-}$ mice was not statistically different from WT mice in either cohort, but Scl-Ab treatment significantly increased the TMD in *Crtap*$^{-/-}$ mice of both cohorts.

Overall, Scl-Ab increased bone mass (BV/TV) at L4 vertebrae in *Crtap*$^{-/-}$ mice from 35% to 72% of WT levels in the wk6–12 cohort, and from 28% to 71% in the wk1–7 cohort. At the

femur, Scl-Ab improved BV/TV from 32% to 100% and from 45% to 69% in the wk6–12 and wk1–7 cohorts, respectively.

Scl-Ab did not affect femur length, but improved cortical femoral parameters in *Crtap*$^{-/-}$ mice

Crtap$^{-/-}$ mouse femurs are shorter than in WT mice (5). In this study, femurs of control *Crtap*$^{-/-}$ mice were on average 11% and 14% shorter than femurs of WT mice in the wk6–12 and wk1–7 cohorts, respectively. Scl-Ab treatment did not significantly affect femur length in either cohort (Table 1). At the center of the femur midshaft, 12 week old control *Crtap*$^{-/-}$ mice showed trends toward impaired cortical geometrical parameters compared with WT mice, including reduced cortical thickness (Ct.Th), cortical bone area (Ct.Ar), anterior-posterior or medio-lateral cross sectional moments of inertia (CSMIs) and diameter; however, the differences were not statistically significant (Table 1). Scl-Ab treatment of *Crtap*$^{-/-}$ mice resulted in significantly increased Ct.Th, Ct.Ar and CSMI a.p., which tended to be even higher than in WT mice. Compared with control *Crtap*$^{-/-}$ mice, femurs of Scl-Ab treated *Crtap*$^{-/-}$ mice showed a trend to increased total cross-sectional area (Tt.Ar), but no substantial change in the marrow area (Ma.Ar), suggesting that Scl-Ab predominantly induced periosteal but not endosteal bone formation. Consistently, in the wk1–7 cohort femoral midshaft Ct.Th, Ct.Ar and CSMI were lower in control *Crtap*$^{-/-}$ mice compared with WT mice, and increased in Scl-Ab treated *Crtap*$^{-/-}$ mice to near WT levels. Similar to the wk6–12 cohort, these increases were accompanied by a trend to increased Tt.Ar (+11%) but no change in Ma.Ar, suggesting that Scl-Ab predominantly induced periosteal bone apposition, but not endosteal bone formation. In the wk6–12 cohort, the TMD of cortical bone of *Crtap*$^{-/-}$ mice was not significantly different from WT mice, but Scl-Ab treatment increased the TMD compared with WT mice. No statistically significant differences of the TMD were observed between groups in the wk1–7 cohort. In summary, while the reduced femur length of *Crtap*$^{-/-}$ mice was not affected by Scl-Ab, sclerostin inhibition improved the impaired cortical parameters at the center of the femur midshaft of *Crtap*$^{-/-}$ mice to WT levels.

Because *Crtap*$^{-/-}$ femurs of the wk1–7 cohort fractured in an unusual pattern during biomechanical testing, with fractures progressing from the midshaft center towards the distal end of the femurs, we also analyzed cortical bone in the distal region of femurs (Supplementary table 1). In the wk1–7 cohort femurs of *Crtap*$^{-/-}$ mice showed a markedly reduced Ct.Th and a lower Ct.Ar compared with WT femurs. Scl-Ab treatment increased Ct.Ar, but did not significantly increase Ct.Th, suggesting that the effects of Scl-Ab on cortical bone of young *Crtap*$^{-/-}$ mice are less robust at distal sites. In contrast, in the wk6–12 cohort Scl-Ab significantly increased the reduced Ct.Th. and Tt.Ar. at the distal femur in *Crtap*$^{-/-}$ mice, accompanied by a trend to a reduced Ma.Ar, suggesting periosteal and endosteal bone apposition. Together, these findings suggest age and site specific differences in the effects of Scl-Ab on cortical bone in *Crtap*$^{-/-}$ mice.

Scl-Ab improved whole bone strength in *Crtap*$^{-/-}$ mice, but not intrinsic bone material properties

Compared with WT mice, femurs of control wk6–12 *Crtap*$^{-/-}$ mice exhibited reduced maximum load, stiffness and energy to failure (65%, 60% and 22% of WT levels, respectively; Table 2). Scl-Ab treatment increased maximum load and stiffness of femurs of *Crtap*$^{-/-}$ mice (to 91% and 88% of WT levels, respectively), but had no significant effect on energy to failure (31% of WT level). At the bone tissue level, ultimate strength and elastic modulus were not significantly different between all three groups, and tended to be lower in control *Crtap*$^{-/-}$ mice compared with WT mice. Toughness was lower in control *Crtap*$^{-/-}$ mice and did not improve with Scl-Ab treatment. While there was no difference in the elastic displacement between all three groups, the post yield displacement, a measure of the bone brittleness, was significantly lower in control and Scl-Ab-treated *Crtap*$^{-/-}$ mice, indicating no effect of Scl-Ab on the increased bone brittleness in *Crtap*$^{-/-}$ mice.

In the wk1–7 age cohort, the evaluation of the femoral biomechanical properties was confounded by an unusual fracture pattern during mechanical loading to failure in both vehicle and Scl-Ab treated *Crtap*$^{-/-}$ mice. While WT femurs fractured transversely at the femur midshaft, in both *Crtap*$^{-/-}$ groups fractures occurred from the midshaft towards the distal end of the femurs. It is likely that the greatly reduced Ct.Th observed in the distal region of femurs of young *Crtap*$^{-/-}$ mice has favored this unusual fracture pattern. Considering these limitations, maximum load, stiffness and energy to failure were lower in control *Crtap*$^{-/-}$ compared with WT mice, and Scl-Ab treatment slightly improved the reduced stiffness, but did not improve maximum load or energy to failure. Ultimate strength, elastic modulus and toughness could not be calculated in a valid way due to the unusual fracture patterns during mechanical loading to failure of both vehicle- and Scl-Ab-treated *Crtap*$^{-/-}$ mice. Femurs of wk1–7 *Crtap*$^{-/-}$ mice showed a greater elastic displacement and a lower post-yield displacement compared with WT mice; Scl-Ab treatment did not result in significant changes in either parameter compared to control *Crtap*$^{-/-}$ mice. Together, Scl-Ab improved maximum load and stiffness in *Crtap*$^{-/-}$ mice of the wk6–12 cohort, but not the wk1–7 cohort, and did not improve the impaired bone tissue properties or the increased brittleness of the bone of *Crtap*$^{-/-}$ mice.

Scl-Ab reduced osteoclast numbers and increased bone formation in *Crtap*$^{-/-}$ mice

Histomorphometry of L4 vertebrae demonstrated that the BV/TV in control *Crtap*$^{-/-}$ mice was reduced to 35–39% the value of WT mice in both age cohorts. Consistent with the microCT results, Scl-Ab treatment of *Crtap*$^{-/-}$ mice almost doubled the BV/TV to 75% of WT mice (Fig. 3). In the wk6–12 cohort, bones of control *Crtap*$^{-/-}$ mice demonstrated increased osteoclast surface (Oc.S/BS), osteoclast numbers (N.Oc/BS), and increased number of osteocytes per bone area (N.Ot/B.Ar) compared with WT mice. The surface and number of osteoblasts (Ob.S/BS and N.Ob/BS) in control *Crtap*$^{-/-}$ mice tended to be higher compared with WT mice, but the difference was not statistically significant. Compared with control *Crtap*$^{-/-}$ mice, Scl-Ab treated *Crtap*$^{-/-}$ mice exhibited reduced Oc.S/BS and N.Oc/BS that were similar to WT levels, but no significant changes in the elevated N.Ot/B.Ar. The absolute osteoclast numbers in the different groups correlated with the TRACP5b serum levels (Supplementary table 2; Pearson correlation coefficient=0.535, p=0.0233).

Ob.S/BS and N.Ob/BS in bones of Scl-Ab treated *Crtap*$^{-/-}$ mice tended to be lower compared with control *Crtap*$^{-/-}$ mice, but the differences were not statistically significant. Similar trends were observed in the wk1–7 cohort, but the differences in Oc.S/BS and N.Ot/B.Ar between control and Scl-Ab treated *Crtap*$^{-/-}$ mice did not reach statistical significance. Dynamic histomorphometry revealed no difference in the mineralizing surface (MS/BS) in control *Crtap*$^{-/-}$ mice compared with WT mice, but showed a reduced mineral apposition rate (MAR) in control *Crtap*$^{-/-}$ mice, resulting in a non-significant trend towards a reduced bone formation rate (BFR/BS). In Scl-Ab treated *Crtap*$^{-/-}$ mice, the MAR was not significantly changed compared with control *Crtap*$^{-/-}$ mice, and still lower than in WT mice; however, in the wk6–12 cohort Scl-Ab treatment increased the MS/BS by 65%, resulting in a 68% increase in BFR compared with control *Crtap*$^{-/-}$ mice, which tended to be higher than in WT mice. In *Crtap*$^{-/-}$ mice of the wk1–7 cohort Scl-Ab was less effective and did not significantly affect MS/BS or BFR. In summary, Scl-Ab normalized the increased osteoclast numbers in *Crtap*$^{-/-}$ mice to WT levels, but did not affect osteoblast numbers or osteocyte density. In *Crtap*$^{-/-}$ mice of the wk6–12 cohort Scl-Ab increased the BFR/BS from 76% to 128% compared with WT mice, but did not significantly affect BFR/BS in the wk1–7 cohort.

Scl-Ab does not affect the lung phenotype in *Crtap*$^{-/-}$ mice

Scl-Ab had no effect on the lung phenotype in *Crtap*$^{-/-}$ mice, as quantified by the distance between alveolar structures. Consistent with earlier results (42,48), control *Crtap*$^{-/-}$ mice in this study exhibited an 8.2μm increase in the mean space between alveolar structures compared with WT mice (Fig. 4). As expected, given the restricted expression pattern of sclerostin, we did not observe a significant effect of sclerostin-inhibition on the lung phenotype of *Crtap*$^{-/-}$ mice, and the MLI of Scl-Ab treated *Crtap*$^{-/-}$ mice was still greater (mean 10.9 μm) compared with WT mice, but not significantly different from control *Crtap*$^{-/-}$ mice.

Discussion

In this study, we demonstrate the beneficial effects of anti-Sclerostin-antibody (Scl-Ab) treatment on the skeleton in a mouse model of recessive Osteogenesis Imperfecta (OI) caused by defects in post-translational collagen modification. We found that 6 weeks of Scl-Ab treatment of *Crtap*$^{-/-}$ mice improved trabecular bone mass and microarchitecture, cortical bone parameters and parameters of bone strength, but did not correct the increased bone brittleness. Both the “young adult” (treatment week 6–12) and “pediatric” (treatment week 1–7) cohorts mostly responded similarly to Scl-Ab administration at trabecular bone, but showed some differences in the response to Scl-Ab in cortical bone. While our findings are largely consistent with the reported beneficial effects of Scl-Ab treatment in mouse models of dominant OI, we also observed certain differences in the response to treatment.

In the trabecular metaphyseal bone of femurs, Scl-Ab administration increased bone mass (BV/TV) and trabecular number (Tb.N) in both age cohorts of *Crtap*$^{-/-}$ mice, and trabecular thickness (Tb.Th) in the wk6–12 cohort. Similar effects of Scl-Ab treatment on femoral trabecular bone have been observed in models of dominant OI, including Brtl/+ mice

(moderate-to-severe OI) treated from 6 months of age for 5 weeks (36), *Col1a2*$^{+/p.G610C}$ mice (moderate OI) treated from 6 weeks for 6 weeks (38), and 4 week old *Col1a1*$^{Jrt/+}$ mice (severe OI) treated for 4 weeks (39). By contrast, femur metaphyseal bone mass was not improved by Scl-Ab in 20 week old *Col1a1*$^{Jrt/+}$ mice treated for 4 weeks (39). The effects of Scl-Ab on trabecular bone in OI mouse spine are less well characterized. While we observed increases in Tb.N, Tb.Th and BV/TV in both age cohorts of *Crtap*$^{-/-}$ mice, no increases in BV/TV were observed in 4 or 20 week old *Col1a1*$^{Jrt/+}$ mice treated for 4 weeks (39). Furthermore, 5 weeks of Scl-Ab treatment did not improve bone mass at the 8th caudal vertebrae in 7 month old Brtl/+ mice (36). However, 10 weeks of Scl-Ab treatment also increased vertebral BV/TV in 5 week old oim/oim mice (40).

At femur midshaft, Scl-Ab injections of *Crtap*$^{-/-}$ mice improved Ct.Th, Ct.Ar and CSMI to WT levels in both age cohorts. These findings are in concordance with the reported Scl-Ab effects in models of dominant OI and oim/oim mice, where treatment has consistently improved the cortical parameters (35–39,41). Overall, these findings suggest mostly beneficial effects of sclerostin inhibition on both trabecular and cortical bone mass in OI models. However, while Scl-Ab increased Ct.Th at the distal femur in *Crtap*$^{-/-}$ mice of the wk6–12 cohort, it did not improve Ct.Th at this location in *Crtap*$^{-/-}$ mice of the younger cohort. This finding could suggest site and age dependent differences in the response of cortical bone to Scl-Ab.

The higher tissue mineral density (TMD) observed in microCT analyses of bones of *Crtap*$^{-/-}$ mice may reflect an increased mineralization of the bone tissue, which has been previously reported in *Crtap*$^{-/-}$ mice and in patients with *CRTAP* mutations using quantitative backscattered electron imaging (49). It has been suggested that the altered morphology, organization and cross-linking of collagen fibers in OI contributes to an increased matrix mineralization by affecting hydroxyapatite crystal size and organization (50–51). The further increase in TMD in trabecular bone of Scl-Ab treated *Crtap*$^{-/-}$ mice likely reflects the robust increases in trabecular thickness, which are known to reduce partial volume effects, thus artificially increasing micro-CT based TMD (45). The increased TMD observed in cortical bone of Scl-Ab treated mice may suggest biological effects of Scl-Ab on cortical mineralization in *Crtap*$^{-/-}$ mice; however, this increase could also be the consequence of reduced partial volume effects resulting from altered cortical porosity (below the resolution of our microCT) and/or the increased cortical thickness.

Biomechanical testing of femurs demonstrated that Scl-Ab treatment improved the biomechanical properties at the whole bone level in 12 week old *Crtap*$^{-/-}$ mice, but did not significantly affect the intrinsic bone tissue properties. In the wk1–7 cohort, Scl-Ab administration was much less effective, and only an increase in stiffness reached statistical significance compared with control *Crtap*$^{-/-}$ mice; however, this may also be influenced by an unusual fracture pattern during biomechanical testing observed in femurs of both Scl-Ab and vehicle treated *Crtap*$^{-/-}$ mice in the wk1–7 cohort. In both age cohorts, we observed no significant effects of Scl-Ab on the greatly reduced post-yield displacement, a parameter associated with brittleness. While our results are consistent with most published studies of sclerostin inhibition in dominant OI mouse models (35–38) and oim/oim mice (41), interesting differences were reported in two studies. First, sclerostin inhibition for 4 weeks

did not improve the maximum load in the *Col1a1*$^{Jrt/+}$ mouse model of severe OI (39). Second, 5 weeks of Scl-Ab treatment increased post-yield displacement in femurs of 7-month old Brtl/+ mice, suggesting an improvement of the brittleness of OI bone (36). Collectively, these data suggest that sclerostin inhibition can improve whole bone strength in most mouse models of OI, and may potentially positively affect the increased brittleness of OI bone. It will have to be determined in future clinical trials, if sclerostin inhibition in OI patients is valuable to improve bone strength and reduce the increased fracture incidence.

Histomorphometry of vertebral bodies of *Crtap*$^{-/-}$ mice demonstrated that Scl-Ab normalized the increased osteoclast numbers to WT levels, but did not significantly affect osteoblast numbers or the increased osteocyte density. Interestingly, Scl-Ab increased Ob.S/BS, but did not significantly affect Oc.S/BS in femurs of *Col1a2*$^{+/p.G610C}$ mice (38). However, in accordance with our observations in *Crtap*$^{-/-}$ mice, Scl-Ab treatment also reduced the elevated Oc.S/BS in ovariectomized rats (29), lowered serum levels of TRACP5b (a marker of osteoclast number) in Brtl/+ mice (36), and reduced serum bone resorption parameters in patients with low BMD (32–33). Dynamic histomorphometry demonstrated no significant effect of Scl-Ab on the reduced MAR in *Crtap*$^{-/-}$ mice, reflecting an osteoblastic defect that cannot be improved by increasing Wnt signaling activity. However, Scl-Ab significantly increased MS/BS by about 65% in the older cohort, resulting in an overall greater BFR/BS. Similar findings with increased MS/BS and BFR/BS were also reported after Scl-Ab treatment of Brtl/+ mice and *Col1a2*$^{+/p.G610C}$ mice (35–36,38). By contrast, Scl-Ab administration did not significantly affect these parameters in the younger *Crtap*$^{-/-}$ mice and at vertebral bodies of 8 and 24 week old *Col1a1*$^{Jrt/+}$ mice, and only improved femoral MS/BS in 24-week, but not 8 week old *Col1a1*$^{Jrt/+}$ mice (39).

Differences among the published studies in dominant OI, and our study, regarding the bone analyzed, analytical methods, severity of OI, mouse genetic background, age and gender, time point analyzed, treatment duration and the Scl-Ab used (Scl-AbVI, this study and (35–37), Scl-AbIII (38) (both from Amgen Inc), BPS804 (39) (Novartis Inc and MorphoSys Inc)) complicate a thorough comparison of the skeletal effects of sclerostin inhibition in OI models. Overall, most evidence in OI models supports that Scl-Ab therapy can improve cortical and trabecular bone mass, improve bone strength, and increase the ratio of osteoblasts to osteoclasts, as well as bone formation. However, the reported differences in the responses to Scl-Ab in OI mouse models also may reflect real differences across skeletal sites, for OI type and severity, age, and gender. If this would be observed in future studies, it may also imply genotype specific approaches for the treatment of OI.

Recently, we found that increased TGF-β signaling is a mechanism contributing to the pathology in models of both dominant and recessive OI, and that TGF-β-inhibition can improve the bone phenotype in both situations (48). Interestingly, while both the TGF-β-inhibiting antibody and Scl-Ab improve trabecular bone mass in *Crtap*$^{-/-}$ mice, sclerostin inhibition seems to be more effective to also increase cortical bone mass compared with TGF-β-inhibition. Of course, different doses of the antibodies and treatment durations may have resulted in different outcomes. It is possible that this difference reflects the differential effects of anti-resorptive vs. bone forming agents on trabecular and cortical bone. However, TGF-β-inhibition also improved the ultimate strength in femurs of *Crtap*$^{-/-}$ mice, while Scl-

Ab treatment did not. Notably, a higher density of osteocytes is present in the bone of more severe forms of OI, and may reflect an impaired bone maturation (52). While Scl-Ab in the current study did not correct the increased osteocyte density in *Crtap*$^{-/-}$ mice, TGF-β-inhibition normalized osteocyte numbers to WT levels, which may contribute to improved bone tissue strength. Furthermore, the WNT and TGF-β signaling pathways interact with each other, for example TGF-β can increase the expression of sclerostin (53–54), and may thereby affect the magnitude of response to Scl-Ab treatment in OI compared to WT mice. It is likely that both pathways differentially affect trabecular vs. cortical bone and bone biomechanical properties in OI, and that the interactions between these and other pathways determine the net outcome of pharmacological interventions targeted at signaling pathways in OI and other bone disorders. Also, this would raise the intriguing possibility that a combinatorial treatment with TGF-β- and sclerostin-inhibitors may be even more beneficial for the therapy of OI, an avenue that may be explored in future studies.

Crtap$^{-/-}$ mice exhibit extraskeletal features, including lung abnormalities, as observed in models of dominant OI (44) and OI patients (44,55–56), including an increased distance of alveolar structures (42). As expected, given the restricted expression pattern of sclerostin, Scl-Ab treatment did not significantly improve the lung phenotype of *Crtap*$^{-/-}$ mice. While this may limit the potential of Scl-Ab therapy as an approach to also target extraskeletal manifestations of OI as compared to anti-TGF-β treatment (48), it may allow for a bone specific therapy of signaling targeted treatments, which may be of advantage in particular in pediatric OI patients, where systemic TGF-β inhibition may also interfere with extraskeletal tissues during growth.

This study has several limitations. First, no blinding to the group assignment (Scl-Ab or PBS only) was possible during treatment, however, the investigators were blinded to genotype and treatment group for the subsequent analyses. Second, recessive OI can be caused by mutations in a variety of genes. While it is possible that Scl-Ab treatment has similar beneficial effects on the skeleton in models of OI caused by mutations in the other two genes of the P3H complex (*Lepre1* and *Ppib*), sclerostin inhibition may have different effects in other forms of recessive OI. Third, the dose of the Scl-Ab used, treatment regimen and duration were chosen based on previous studies in animal models. It is possible that different treatment regimens may differently affect the evaluated bone tissues. Also, a longer treatment duration may have further improved the trabecular bone parameters. Fourth, from a translational perspective, the dose and treatment interval used in *Crtap*$^{-/-}$ mice are different from those currently explored in human clinical trials (33) and the optimal Scl-Ab dosage, treatment interval and duration still has to be established for OI patients. Finally, in this study we only treated female *Crtap*$^{-/-}$ mice, and it is possible that sclerostin-inhibition differentially affects male *Crtap*$^{-/-}$ mice.

In conclusion, Scl-Ab treatment improved bone mass, trabecular microarchitecture, parameters of bone strength and bone formation, while it decreased osteoclast numbers in *Crtap*$^{-/-}$ mice, a model of recessive OI. Notably, the effects of Scl-Ab on bone strength and bone formation were much less robust in the younger cohort, suggesting age dependent differences in response. These findings could translate to OI caused by mutations in other members of the P3H1 complex in mouse models and in patients with recessive OI. While

our findings are mostly consistent with the findings in mouse models of dominant OI, certain aspects of the bone architecture and cellular activity seem to be differentially affected by sclerostin inhibition in recessive OI due to Crtap deficiency. Overall, based on our study and the published work in models of dominant OI, Scl-Ab treatment seems to be a promising new avenue for the treatment of OI patients. Ultimately, it will have to be determined in future clinical trials, if Scl-Ab therapy is safe and effective in adult and pediatric OI patients, and if potential differences in response to treatment could justify a genotype specific approach to therapy in OI.

Supplementary Material

Refer to Web version on PubMed Central for supplementary material.

Acknowledgments

We like to thank M. Bagos and C. Jiang for help with microCT analyses, and M. Starbuck (MD Anderson Cancer Center) for consultation and advice in bone histomorphometry. In addition, we want to thank R. Morello and D. Baldridge for helpful discussions, and P. Fonseca for editorial assistance. Franklin Asuncion and Michael S Ominsky are employees of Amgen Inc., Hua Zhu Ke is an employee of UCB Pharma. None of the other authors have any conflicts of interest to declare. This work was supported by the following funding sources: a research grant from the German Research Foundation/Deutsche Forschungsgemeinschaft (I.G.), a Michael Geisman Fellowship from the Osteogenesis Imperfecta Foundation (I.G.), NIH grants 1F31DE024693-01 (S.A.), 5F31DE022483 (C.L), 5F31DE020954 (E.H), P01 HD70394 (B.L.) and U54 AR068069 (B.L.). Additionally, this work was supported by a pilot grant from The Rolanette and Berdon Lawrence Bone Disease Program of Texas (T.Y.) and the Howard Hughes Medical Institute Foundation (B.L.). This work was also supported by the BCM Intellectual and Developmental Disabilities Research Center (HD024064) from the Eunice Kennedy Shriver National Institute Of Child Health & Human Development, the BCM Advanced Technology Cores with funding from the NIH (AI036211, CA125123, and RR024574), the Rolanette and Berdon Lawrence Bone Disease Program of Texas, and the BCM Center for Skeletal Medicine and Biology.

References

1. Rauch F, Glorieux FH. Osteogenesis imperfecta. Lancet. 2004; 363(9418):1377–1385. [PubMed: 15110498]
2. Byers PH, Pyott SM. Recessively inherited forms of osteogenesis imperfecta. Annu Rev Genet. 2012; 46:475–497. [PubMed: 23145505]
3. Ishikawa Y, Wirz J, Vranka JA, Nagata K, Bachinger HP. Biochemical characterization of the prolyl 3-hydroxylase 1.cartilage-associated protein.cyclophilin B complex. J Biol Chem. 2009; 284(26): 17641–17647. [PubMed: 19419969]
4. Vranka JA, Sakai LY, Bachinger HP. Prolyl 3-hydroxylase 1, enzyme characterization and identification of a novel family of enzymes. J Biol Chem. 2004; 279(22):23615–23621. [PubMed: 15044469]
5. Morello R, Bertin TK, Chen Y, Hicks J, Tonachini L, Monticone M, Castagnola P, Rauch F, Glorieux FH, Vranka J, Bachinger HP, Pace JM, Schwarze U, Byers PH, Weis M, Fernandes RJ, Eyre DR, Yao Z, Boyce BF, Lee B. CRTAP is required for prolyl 3- hydroxylation and mutations cause recessive osteogenesis imperfecta. Cell. 2006; 127(2):291–304. [PubMed: 17055431]
6. Baldridge D, Schwarze U, Morello R, Lennington J, Bertin TK, Pace JM, Pepin MG, Weis M, Eyre DR, Walsh J, Lambert D, Green A, Robinson H, Michelson M, Houge G, Lindman C, Martin J, Ward J, Lemyre E, Mitchell JJ, Krakow D, Rimoin DL, Cohn DH, Byers PH, Lee B. CRTAP and LEPRE1 mutations in recessive osteogenesis imperfecta. Hum Mutat. 2008; 29(12):1435–1442. [PubMed: 18566967]
7. Barnes AM, Chang W, Morello R, Cabral WA, Weis M, Eyre DR, Leikin S, Makareeva E, Kuznetsova N, Uveges TE, Ashok A, Flor AW, Mulvihill JJ, Wilson PL, Sundaram UT, Lee B, Marini JC. Deficiency of cartilage-associated protein in recessive lethal osteogenesis imperfecta. N Engl J Med. 2006; 355(26):2757–2764. [PubMed: 17192541]

8. Pyott SM, Schwarze U, Christiansen HE, Pepin MG, Leistritz DF, Dineen R, Harris C, Burton BK, Angle B, Kim K, Sussman MD, Weis M, Eyre DR, Russell DW, McCarthy KJ, Steiner RD, Byers PH. Mutations in PPIB (cyclophilin B) delay type I procollagen chain association and result in perinatal lethal to moderate osteogenesis imperfecta phenotypes. Hum Mol Genet. 2011; 20(8): 1595–1609. [PubMed: 21282188]

9. Glorieux FH, Bishop NJ, Plotkin H, Chabot G, Lanoue G, Travers R. Cyclic administration of pamidronate in children with severe osteogenesis imperfecta. N Engl J Med. 1998; 339(14):947–952. [PubMed: 9753709]

10. Rauch F, Plotkin H, Zeitlin L, Glorieux FH. Bone mass, size, and density in children and adolescents with osteogenesis imperfecta: effect of intravenous pamidronate therapy. J Bone Miner Res. 2003; 18(4):610–614. [PubMed: 12674321]

11. Falk MJ, Heeger S, Lynch KA, DeCaro KR, Bohach D, Gibson KS, Warman ML. Intravenous bisphosphonate therapy in children with osteogenesis imperfecta. Pediatrics. 2003; 111(3):573–578. [PubMed: 12612238]

12. Gatti D, Antoniazzi F, Prizzi R, Braga V, Rossini M, Tato L, Viapiana O, Adami S. Intravenous neridronate in children with osteogenesis imperfecta: a randomized controlled study. J Bone Miner Res. 2005; 20(5):758–763. [PubMed: 15824848]

13. Letocha AD, Cintas HL, Troendle JF, Reynolds JC, Cann CE, Chernoff EJ, Hill SC, Gerber LH, Marini JC. Controlled trial of pamidronate in children with types III and IV osteogenesis imperfecta confirms vertebral gains but not short-term functional improvement. J Bone Miner Res. 2005; 20(6):977–986. [PubMed: 15883638]

14. Ward LM, Rauch F, Whyte MP, D'Astous J, Gates PE, Grogan D, Lester EL, McCall RE, Pressly TA, Sanders JO, Smith PA, Steiner RD, Sullivan E, Tyerman G, Smith-Wright DL, Verbruggen N, Heyden N, Lombardi A, Glorieux FH. Alendronate for the treatment of pediatric osteogenesis imperfecta: a randomized placebo-controlled study. J Clin Endocrinol Metab. 2011; 96(2):355–364. [PubMed: 21106710]

15. Shi CG, Zhang Y, Yuan W. Efficacy of Bisphosphonates on Bone Mineral Density and Fracture Rate in Patients With Osteogenesis Imperfecta: A Systematic Review and Meta-analysis. Am J Ther. 2015

16. Rauch F, Munns CF, Land C, Cheung M, Glorieux FH. Risedronate in the treatment of mild pediatric osteogenesis imperfecta: a randomized placebo-controlled study. J Bone Miner Res. 2009; 24(7):1282–1289. [PubMed: 19257821]

17. Adami S, Gatti D, Colapietro F, Fracassi E, Braga V, Rossini M, Tato L. Intravenous neridronate in adults with osteogenesis imperfecta. J Bone Miner Res. 2003; 18(1):126–130. [PubMed: 12510813]

18. Chevrel G, Schott AM, Fontanges E, Charrin JE, Lina-Granade G, Duboeuf F, Garnero P, Arlot M, Raynal C, Meunier PJ. Effects of oral alendronate on BMD in adult patients with osteogenesis imperfecta: a 3-year randomized placebo-controlled trial. J Bone Miner Res. 2006; 21(2):300–306. [PubMed: 16418786]

19. Hoyer-Kuhn H, Semler O, Schoenau E. Effect of denosumab on the growing skeleton in osteogenesis imperfecta. J Clin Endocrinol Metab. 2014; 99(11):3954–3955. [PubMed: 25148238]

20. Hoyer-Kuhn H, Netzer C, Koerber F, Schoenau E, Semler O. Two years' experience with denosumab for children with osteogenesis imperfecta type VI. Orphanet J Rare Dis. 2014; 9:145. [PubMed: 25257953]

21. Neer RM, Arnaud CD, Zanchetta JR, Prince R, Gaich GA, Reginster JY, Hodsman AB, Eriksen EF, Ish-Shalom S, Genant HK, Wang O, Mitlak BH. Effect of parathyroid hormone (1–34) on fractures and bone mineral density in postmenopausal women with osteoporosis. N Engl J Med. 2001; 344(19):1434–1441. [PubMed: 11346808]

22. Orwoll ES, Shapiro J, Veith S, Wang Y, Lapidus J, Vanek C, Reeder JL, Keaveny TM, Lee DC, Mullins MA, Nagamani SC, Lee B. Evaluation of teriparatide treatment in adults with osteogenesis imperfecta. J Clin Invest. 2014; 124(2):491–498. [PubMed: 24463451]

23. Vahle JL, Sato M, Long GG, Young JK, Francis PC, Engelhardt JA, Westmore MS, Linda Y, Nold JB. Skeletal changes in rats given daily subcutaneous injections of recombinant human parathyroid hormone (1–34) for 2 years and relevance to human safety. Toxicol Pathol. 2002; 30(3):312–321. [PubMed: 12051548]

24. van Bezooijen RL, Roelen BA, Visser A, van der Wee-Pals L, de Wilt E, Karperien M, Hamersma H, Papapoulos SE, ten Dijke P, Lowik CW. Sclerostin is an osteocyte-expressed negative regulator of bone formation, but not a classical BMP antagonist. J Exp Med. 2004; 199(6):805–814. [PubMed: 15024046]
25. Poole KE, van Bezooijen RL, Loveridge N, Hamersma H, Papapoulos SE, Lowik CW, Reeve J. Sclerostin is a delayed secreted product of osteocytes that inhibits bone formation. FASEB J. 2005; 19(13):1842–1844. [PubMed: 16123173]
26. Li X, Zhang Y, Kang H, Liu W, Liu P, Zhang J, Harris SE, Wu D. Sclerostin binds to LRP5/6 and antagonizes canonical Wnt signaling. J Biol Chem. 2005; 280(20):19883–19887. [PubMed: 15778503]
27. Sutherland MK, Geoghegan JC, Yu C, Turcott E, Skonier JE, Winkler DG, Latham JA. Sclerostin promotes the apoptosis of human osteoblastic cells: a novel regulation of bone formation. Bone. 2004; 35(4):828–835. [PubMed: 15454089]
28. Baron R, Kneissel M. WNT signaling in bone homeostasis and disease: from human mutations to treatments. Nat Med. 2013; 19(2):179–192. [PubMed: 23389618]
29. Li X, Ominsky MS, Warmington KS, Morony S, Gong J, Cao J, Gao Y, Shalhoub V, Tipton B, Haldankar R, Chen Q, Winters A, Boone T, Geng Z, Niu QT, Ke HZ, Kostenuik PJ, Simonet WS, Lacey DL, Paszty C. Sclerostin antibody treatment increases bone formation, bone mass, and bone strength in a rat model of postmenopausal osteoporosis. Journal of bone and mineral research : the official journal of the American Society for Bone and Mineral Research. 2009; 24(4):578–588.
30. Li X, Warmington KS, Niu QT, Asuncion FJ, Barrero M, Grisanti M, Dwyer D, Stouch B, Thway TM, Stolina M, Ominsky MS, Kostenuik PJ, Simonet WS, Paszty C, Ke HZ. Inhibition of sclerostin by monoclonal antibody increases bone formation, bone mass, and bone strength in aged male rats. Journal of bone and mineral research : the official journal of the American Society for Bone and Mineral Research. 2010; 25(12):2647–2656.
31. Tian X, Jee WS, Li X, Paszty C, Ke HZ. Sclerostin antibody increases bone mass by stimulating bone formation and inhibiting bone resorption in a hindlimb-immobilization rat model. Bone. 2011; 48(2):197–201. [PubMed: 20850580]
32. Padhi D, Allison M, Kivitz AJ, Gutierrez MJ, Stouch B, Wang C, Jang G. Multiple doses of sclerostin antibody romosozumab in healthy men and postmenopausal women with low bone mass: a randomized, double-blind, placebo-controlled study. J Clin Pharmacol. 2014; 54(2):168–178. [PubMed: 24272917]
33. McClung MR, Grauer A, Boonen S, Bolognese MA, Brown JP, Diez-Perez A, Langdahl BL, Reginster JY, Zanchetta JR, Wasserman SM, Katz L, Maddox J, Yang YC, Libanati C, Bone HG. Romosozumab in postmenopausal women with low bone mineral density. The New England journal of medicine. 2014; 370(5):412–420. [PubMed: 24382002]
34. McColm J, Hu L, Womack T, Tang CC, Chiang AY. Single- and multiple-dose randomized studies of blosozumab, a monoclonal antibody against sclerostin, in healthy postmenopausal women. J Bone Miner Res. 2014; 29(4):935–943. [PubMed: 23996473]
35. Sinder BP, Eddy MM, Ominsky MS, Caird MS, Marini JC, Kozloff KM. Sclerostin antibody improves skeletal parameters in a Brtl/+ mouse model of osteogenesis imperfecta. J Bone Miner Res. 2013; 28(1):73–80. [PubMed: 22836659]
36. Sinder BP, White LE, Salemi JD, Ominsky MS, Caird MS, Marini JC, Kozloff KM. Adult Brtl/+ mouse model of osteogenesis imperfecta demonstrates anabolic response to sclerostin antibody treatment with increased bone mass and strength. Osteoporos Int. 2014; 25(8):2097–2107. [PubMed: 24803333]
37. Sinder BP, Salemi JD, Ominsky MS, Caird MS, Marini JC, Kozloff KM. Rapidly growing Brtl/+ mouse model of osteogenesis imperfecta improves bone mass and strength with sclerostin antibody treatment. Bone. 2015; 71:115–123. [PubMed: 25445450]
38. Jacobsen CM, Barber LA, Ayturk UM, Roberts HJ, Deal LE, Schwartz MA, Weis M, Eyre D, Zurakowski D, Robling AG, Warman ML. Targeting the LRP5 pathway improves bone properties in a mouse model of osteogenesis imperfecta. J Bone Miner Res. 2014; 29(10):2297–2306. [PubMed: 24677211]

39. Roschger A, Roschger P, Keplingter P, Klaushofer K, Abdullah S, Kneissel M, Rauch F. Effect of sclerostin antibody treatment in a mouse model of severe osteogenesis imperfecta. Bone. 2014; 66:182–188. [PubMed: 24953712]
40. Chappard D, Ammann P, Ominsky M, Behets C, Devogelaer JP, Manicourt DH. Sclerostin neutralizing monoclonal antibody decreased significantly the number of pelvic fractures and improves dramatically the size and interconnectivity of lumbar trabecular bone in oim/oim mice. Abstract ECTS meeting. 2012
41. Devogelaer P, Ammann P, Ominsky M, Behets C, Manicourt D. Effects of Sclerostin Antibody on Tissue Level Strength in oim Mice. Abstact ASBMR meeting. 2012
42. Baldridge D, Lennington J, Weis M, Homan EP, Jiang MM, Munivez E, Keene DR, Hogue WR, Pyott S, Byers PH, Krakow D, Cohn DH, Eyre DR, Lee B, Morello R. Generalized connective tissue disease in Crtap−/− mouse. PLoS One. 2010; 5(5):e10560. [PubMed: 20485499]
43. McAllion SJ, Paterson CR. Causes of death in osteogenesis imperfecta. J Clin Pathol. 1996; 49(8): 627–630. [PubMed: 8881910]
44. Thiele F, Cohrs CM, Flor A, Lisse TS, Przemeck GK, Horsch M, Schrewe A, Gailus-Durner V, Ivandic B, Katus HA, Wurst W, Reisenberg C, Chaney H, Fuchs H, Hans W, Beckers J, Marini JC, Hrabe de Angelis M. Cardiopulmonary dysfunction in the Osteogenesis imperfecta mouse model Aga2 and human patients are caused by bone-independent mechanisms. Hum Mol Genet. 2012; 21(16):3535–3545. [PubMed: 22589248]
45. Bouxsein ML, Boyd SK, Christiansen BA, Guldberg RE, Jepsen KJ, Muller R. Guidelines for assessment of bone microstructure in rodents using micro-computed tomography. J Bone Miner Res. 2010; 25(7):1468–1486. [PubMed: 20533309]
46. Turner CH, Burr DB. Basic biomechanical measurements of bone: a tutorial. Bone. 1993; 14(4): 595–608. [PubMed: 8274302]
47. Chen ZH, Lam HC, Jin Y, Kim HP, Cao J, Lee SJ, Ifedigbo E, Parameswaran H, Ryter SW, Choi AM. Autophagy protein microtubule-associated protein 1 light chain-3B (LC3B) activates extrinsic apoptosis during cigarette smoke-induced emphysema. Proc Natl Acad Sci U S A. 2010; 107(44):18880–18885. [PubMed: 20956295]
48. Grafe I, Yang T, Alexander S, Homan EP, Lietman C, Jiang MM, Bertin T, Munivez E, Chen Y, Dawson B, Ishikawa Y, Weis MA, Sampath TK, Ambrose C, Eyre D, Bachinger HP, Lee B. Excessive transforming growth factor-beta signaling is a common mechanism in osteogenesis imperfecta. Nat Med. 2014; 20(6):670–675. [PubMed: 24793237]
49. Fratzl-Zelman N, Morello R, Lee B, Rauch F, Glorieux FH, Misof BM, Klaushofer K, Roschger P. CRTAP deficiency leads to abnormally high bone matrix mineralization in a murine model and in children with osteogenesis imperfecta type VII. Bone. 2010; 46(3):820–826. [PubMed: 19895918]
50. Eyre DR, Weis MA. Bone collagen: new clues to its mineralization mechanism from recessive osteogenesis imperfecta. Calcif Tissue Int. 2013; 93(4):338–347. [PubMed: 23508630]
51. Bart ZR, Hammond MA, Wallace JM. Multi-scale analysis of bone chemistry, morphology and mechanics in the oim model of osteogenesis imperfecta. Connect Tissue Res. 2014; 55(Suppl 1):4–8. [PubMed: 25158170]
52. Sarathchandra P, Pope FM, Kayser MV, Ali SY. A light and electron microscopic study of osteogenesis imperfecta bone samples, with reference to collagen chemistry and clinical phenotype. J Pathol. 2000; 192(3):385–395. [PubMed: 11054723]
53. Loots GG, Keller H, Leupin O, Murugesh D, Collette NM, Genetos DC. TGF-beta regulates sclerostin expression via the ECR5 enhancer. Bone. 2012; 50(3):663–669. [PubMed: 22155511]
54. Nguyen J, Tang SY, Nguyen D, Alliston T. Load regulates bone formation and Sclerostin expression through a TGFbeta-dependent mechanism. PLoS One. 2013; 8(1):e53813. [PubMed: 23308287]
55. Shapiro JR, Burn VE, Chipman SD, Jacobs JB, Schloo B, Reid L, Larsen N, Louis F. Pulmonary hypoplasia and osteogenesis imperfecta type II with defective synthesis of alpha I(1) procollagen. Bone. 1989; 10(3):165–171. [PubMed: 2803853]
56. Widmann RF, Bitan FD, Laplaza FJ, Burke SW, DiMaio MF, Schneider R. Spinal deformity, pulmonary compromise, and quality of life in osteogenesis imperfecta. Spine (Phila Pa 1976). 1999; 24(16):1673–1678. [PubMed: 10472101]

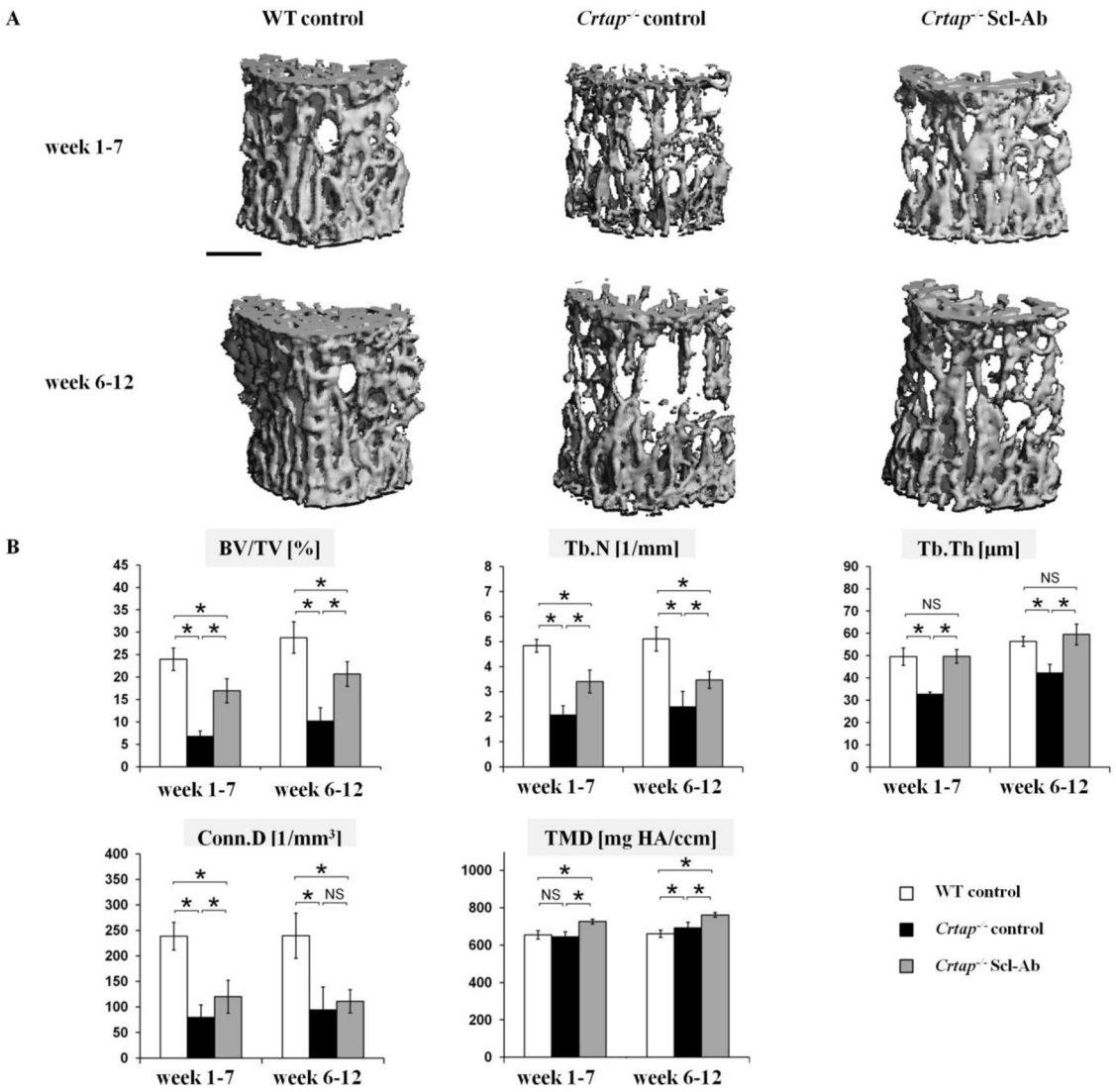

Fig. 1.

Scl-Ab treatment improved trabecular bone mass and microarchitectural parameters at vertebrae in *Crtap*$^{-/-}$ mice. (A) MicroCT reconstructions of trabecular bone at L4 vertebral bodies. Mice were treated with either PBS (wild type (WT) and control *Crtap*$^{-/-}$ mice) or Scl-Ab (*Crtap*$^{-/-}$ mice). (scale bar=500µm). (B) MicroCT analysis results of L4 vertebrae for bone volume/total volume (BV/TV), trabecular number (Tb.N), trabecular thickness (Tb.Th), connectivity density (Conn.D) and tissue mineral density (TMD) in WT, control *Crtap*$^{-/-}$ mice and Scl-Ab treated *Crtap*$^{-/-}$ mice treated from week 6–12 and from week 1–7. Results are shown as means ± SD; n=7 per group. *p<0.05 between indicated groups, NS=not significant.

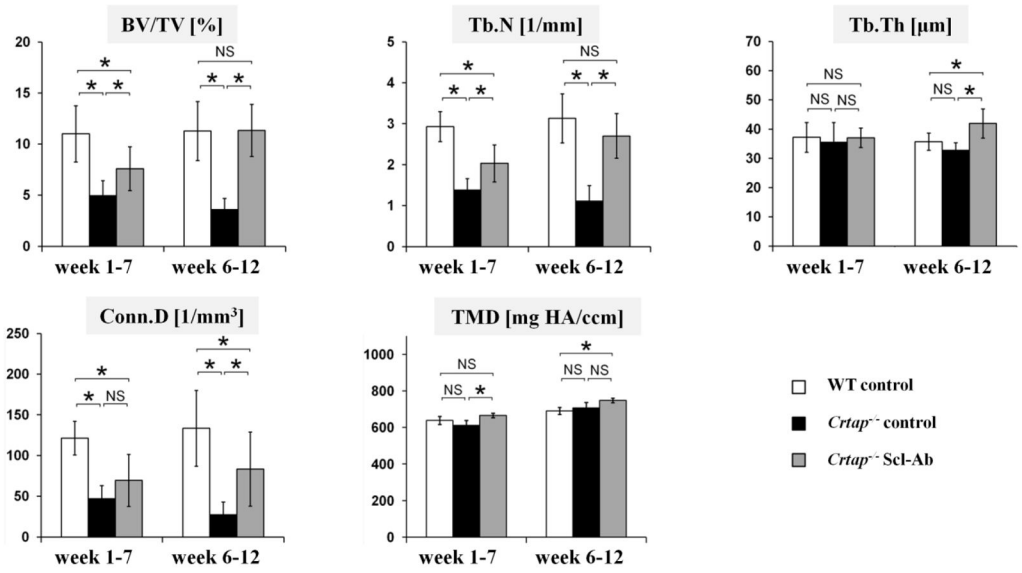

Fig. 2.

Scl-Ab treatment improved trabecular bone mass and microarchitectural parameters at the femur metaphysis in *Crtap*$^{-/-}$ mice. MicroCT analysis of the distal metaphysis for bone volume/total volume (BV/TV), trabecular number (Tb.N), trabecular thickness (Tb.Th), connectivity density (Conn.D) and tissue mineral density (TMD) in WT, control *Crtap*$^{-/-}$ mice and Scl-Ab treated *Crtap*$^{-/-}$ mice treated from week 6–12 and from week 1–7. Results are shown as means ± SD. In week 6–12 cohort n=7 per group, in week 1–7 cohort n=7 per group for WT and *Crtap*$^{-/-}$ Scl-Ab, n=6 for *Crtap*$^{-/-}$ control. *p<0.05 between indicated groups, NS=not significant.

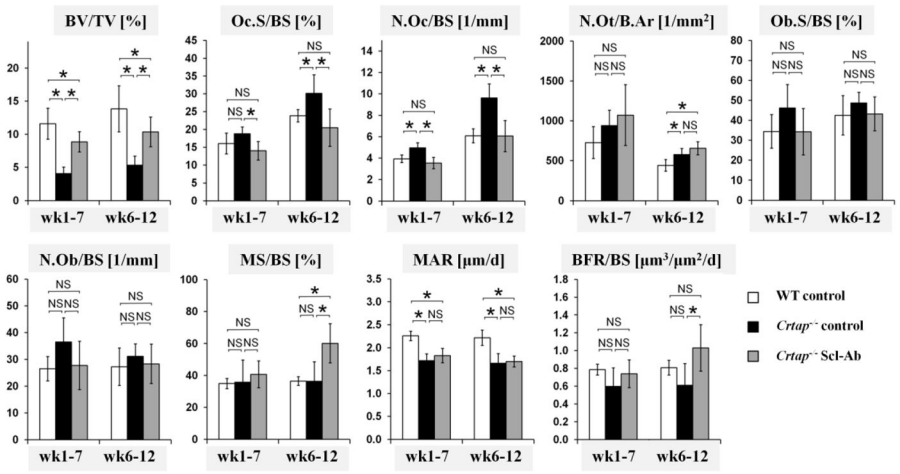

Fig. 3.

Histomorphometry analysis of vertebrae L4 of WT, control *Crtap*$^{-/-}$ mice and Scl-Ab treated *Crtap*$^{-/-}$ mice. Shown are bone volume/total volume (BV/TV), osteoclast surface/bone surface (Oc.S/BS), osteoclast number/bone surface (N.Oc/BS), osteocyte number/bone area (N.Ot/B.Ar), osteoblast surface/bone surface (Ob.S/BS), osteoblast number/bone surface (N.Ob/BS), mineralizing surface/bone surface (MS/BS), mineral apposition rate (MAR) and bone formation rate/bone surface (BFR/BS). Data are shown as means ± SD, n=6 per group. *p<0.05 between indicated groups, NS=not significant.

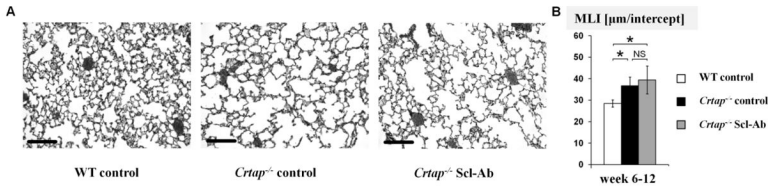

Fig. 4.

Scl-Ab did not affect the lung phenotype of *Crtap*$^{-/-}$ mice. (A) representative images of H&E stained sections from inflated lungs of WT, control *Crtap*$^{-/-}$ mice and Scl-Ab treated *Crtap*$^{-/-}$ mice that were treated from week 6–12 (20X magnification, scale bars=100µm). (B) Quantification of the distance between alveolar structures in lung sections using the mean linear intercept method (MLI). Results are shown for WT, control *Crtap*$^{-/-}$ mice and Scl-Ab treated *Crtap*$^{-/-}$ mice that were treated from week 6–12. Data is presented as means ± SD. N=8 for WT mice, n=6 for control *Crtap*$^{-/-}$ mice and Scl-Ab *Crtap*$^{-/-}$ mice (10 images analyzed per mouse). *$p<0.05$ between indicated groups, NS=not significant.

Table 1

Femur length and cortical microCT parameters at femur center

	Wild type		*Crtap*$^{-/-}$ control		*Crtap*$^{-/-}$ Scl-Ab		ANOVA
	mean	**SD**	**mean**	**SD**	**mean**	**SD**	***P* value**
Week 6–12 cohort							
Femur length [mm]	**15.13**	0.10	**13.45**	0.38^{+}	**13.63**	0.34$^{\#}$	**<0.001**
Cortical thickness [mm]	**0.216**	0.013	**0.199**	0.021	**0.253**	0.020$^{\#*}$	**<0.001**
Cortical bone area [mm^2]	**0.879**	0.087	**0.791**	0.107	**1.040**	0.113*	**0.004**
Marrow area [mm^2]	**0.884**	0.094	**0.879**	0.122	**0.827**	0.139	**0.632**
Total cross-sectional area [mm^2]	**1.782**	0.172	**1.689**	0.197	**1.888**	0.224	**0.226**
CSMI m.l. [mm^4]	**0.251**	0.042	**0.215**	0.052	**0.316**	0.071*	**0.015**
CSMI a.p. [mm^4]	**0.151**	0.029	**0.132**	0.030	**0.174**	0.039	**0.103**
Diameter a.p. [mm]	**1.286**	0.077	**1.241**	0.069	**1.299**	0.088	**0.404**
TMD [mg HA/ccm]	**1020**	27	**1040**	29	**1078**	20$^{\#*}$	**0.002**
Week 1–7 cohort							
Femur length [mm]	**14.51**	0.34	**12.55**	0.45^{+}	**12.33**	0.33$^{\#}$	**<0.001**
Cortical thickness [mm]	**0.176**	0.007	**0.137**	0.011^{+}	**0.173**	0.024*	**0.003**
Cortical bone area [mm^2]	**0.689**	0.038	**0.539**	0.044^{+}	**0.714**	0.108*	**0.003**
Marrow area [mm^2]	**0.862**	0.092	**0.972**	0.082	**0.972**	0.110	**0.076**
Total cross-sectional area [mm^2]	**1.565**	0.116	**1.527**	0.098	**1.703**	0.151	**0.046**
CSMI m.l. [mm^4]	**0.176**	0.022	**0.142**	0.017	**0.213**	0.047*	**0.004**
CSMI a.p. [mm^4]	**0.113**	0.014	**0.086**	0.010^{+}	**0.120**	0.022*	**0.004**
Diameter a.p. [mm]	**1.238**	0.049	**1.210**	0.023	**1.285**	0.051*	**0.029**
TMD [mg HA/ccm]	**952**	10	**934**	35	**948**	19	**0.368**

N=7 for WT and *Crtap*$^{-/-}$ Scl-Ab, N=6 for *Crtap*$^{-/-}$ control in both cohorts. CSMI=cross sectional moment of inertia, m.l.=medio-lateral, a.p.=anterior-posterior, TMD=tissue mineral density.

$^{+}$p < 0.05 WT vs. control *Crtap*$^{-/-}$

$^{\#}$p < 0.05 WT vs. Scl-Ab *Crtap*$^{-/-}$

*p < 0.05 control *Crtap*$^{-/-}$ vs. Scl-Ab *Crtap*$^{-/-}$

Table 2

Biomechanical properties of femurs

	Wild type		*Crtap*$^{-/-}$ control		*Crtap*$^{-/-}$ Scl-Ab		ANOVA
	mean	**SD**	**mean**	**SD**	**mean**	**SD**	***P* value**
Week 6–12 cohort							
Maximum load [N]	**21.60**	2.26	**14.02**	1.41^{+}	**19.70**	3.70*	**0.006**
Stiffness [N/mm]	**147.2**	9.3	**88.0**	27.2^{+}	**130.1**	20.5*	**0.008**
Energy to failure [N*mm]	**8.78**	2.46	**1.96**	0.74^{+}	**2.72**	1.18	**0.010**
Ultimate strength [MPa]	**183.9**	10.4	**141.1**	23.9	**146.3**	30.7	**0.094**
Elastic modulus [GPa]	**6.29**	1.67	**4.46**	1.67	**4.54**	0.92	**0.209**
Toughness to failure [MPa]	**14.99**	2.11	**3.87**	1.15^{+}	**4.27**	1.80$^{\#}$	**<0.001**
Elastic displacement [mm]	**0.180**	0.020	**0.184**	0.021	**0.178**	0.028	**0.919**
Post-yield displacement [mm]	**0.360**	0.101	**0.051**	0.070^{+}	**0.047**	0.048$^{\#}$	**<0.001**
Week 1–7 cohort							
Maximum load [N]	**13.06**	2.02	**6.64**	1.24^{+}	**7.79**	1.36$^{\#}$	**<0.001**
Stiffness [N/mm]	**80.0**	12.0	**36.3**	9.0^{+}	**49.2**	7.6$^{\#*}$	**<0.001**
Energy to failure [N*mm]	**5.20**	1.19	**1.05**	0.42^{+}	**1.04**	0.11$^{\#}$	**<0.001**
Ultimate strength [MPa]	*N/A*		*N/A*		*N/A*		
Elastic modulus [GPa]	*N/A*		*N/A*		*N/A*		
Toughness to failure [MPa]	*N/A*		*N/A*		*N/A*		
Elastic displacement [mm]	**0.113**	0.018	**0.162**	0.021^{+}	**0.145**	0.029	**0.004**
Post-yield displacement [mm]	**0.411**	0.062	**0.075**	0.070^{+}	**0.068**	0.047$^{\#}$	**<0.001**

N=3 for WT, N=5 for *Crtap*$^{-/-}$ control and *Crtap*$^{-/-}$ Scl-Ab in the week 6–12 cohort, N=9 for WT, N=6 for *Crtap*$^{-/-}$ control and *Crtap*$^{-/-}$ Scl-Ab in the week 1–7 cohort, *N/A*=not applicable.

$^{+}$p < 0.05 WT vs. control *Crtap*$^{-/-}$

$^{\#}$p < 0.05 WT vs. Scl-Ab *Crtap*$^{-/-}$

*p < 0.05 control *Crtap*$^{-/-}$ vs. Scl-Ab *Crtap*$^{-/-}$